Supporting Information

Vacancy-Induced Asymmetric Coordination of Single-Atom Bismuth for Selective Photoelectrochemical Oxidation of Glycerol to Dihydroxyacetone

Xinyan Feng[a,b1], Qisheng Zang[a1], Tingting Sun[a], Xuefan Feng[a], Junliang Liu[a], Hao Yu[a], Yu Yang[a], Fuqin Zhang[a]*

[a] Powder Metallurgy Research Institute, Central South University, Changsha 410083, PR China

[b] School of Materials Science and Engineering (MSE), NingboTech University, Ningbo 315211, China

* Corresponding authors: Fuqin Zhang, E-mail: zhangfuqin@csu.edu.cn

[1] These authors contributed equally

Experimental Section

Chemicals and materials

Ammonium metatungstate ($(NH_4)_6H_2W_{12}O_{40}•xH_2O$, AR, ≥99.5%), bismuth (III) nitrate pentahydrate ($Bi(NO_3)_3•5H_2O$, AR, ≥99.5%), ethylene glycol ($C_2H_6O_2$, AR, 99.5%) and glycerol ($C_3H_8O_3$, AR, 99.5%) were purchased from Macklin Reagent Co., ltd. Sulfuric acid (H_2SO_4, AR, 98%), hydrochloric acid (HCl, AR, 37%), sodium sulfate (Na_2SO_4, AR, ≥99.5%), citric acid ($C_6H_8O_7$, AR, ≥99.5%) and ethanol (C_2H_6O, AR, 99.5%) were obtained from Sinopharm Chemical Reagent Co., Ltd. All the reagents were used without further purification.

Fabrication of WO_3 photoanode

The WO_3 photoanode was fabricated by a facile drop casting method. 0.2 mmol $(NH_4)_6H_2W_{12}O_{40}$, 1.5 mmol citric acid and 1 ml HCl (3M) were dissolved in 15 ml deionized water and stirred for 30 min at room temperature to prepare the precursor solution. 40 μL of the as-prepared solution was dropped onto clean fluorine-doped tin oxide glass (FTO) and then dried at 60 °C. Then, the above FTO was annealed in a box furnace at 500 °C for 120 min in air and cooled to room temperature (RT) to obtained WO_3 photoanode.

Fabrication of Bi-WO_3 photoanode

For Bi-WO_3, the ion exchange process was needed. Typically, 10 mg of bismuth (III) nitrate pentahydrate ($Bi(NO_3)_3•5H_2O$) was dissolved in 20 mL of ethylene glycol, and WO_3 photoanode was immersed in the above mentioned clear solution for 3 h. The dried photoanode was annealed in a box furnace at 500 °C for 30 min in air and cooled to RT to obtained Bi-WO_3 photoanode.

Fabrication of Bi-N/WO_3 photoanodes

Bi-N/WO_3 photoanode was prepared by treating Bi-WO_3 photoanode with high temperature ammonia gas. The Bi-WO_3 sample synthesized in the above steps was annealed in 10%NH_3 atmosphere at 300℃ for 20 min in a box furnace to obtain Bi,N-WO_3 photoanode.

Characterizations

Scanning Electron Microscope (SEM) images were acquired on a Helios Nanolab 600i (FEI) operated at 2 kV. HAADF STEM images were taken on a spherical aberration-corrected TEM (Thermo Fisher Spectra 300) equipped with an Energy Dispersive X-Ray Analyzer (EDX). X-ray powder diffraction (XRD) motifs of the photoanodes were recorded on an X-ray diffractometer (XRD, D/MAX2550PC, Rigaku) with Cu-Kα radiation. X-ray photoelectron spectroscopy (XPS) was collected on Thermo Fisher Scientific spectrometer and the spectra were calibrated with C 1s at 284.6 eV. UV-Vis diffuse reflectance spectra (DRS) were recorded on a Shimadzu UV-3600 spectrophotometer in the range of 200-800 nm with $BaSO_4$ as the standard reflectance material. The bandgap of sample was converted based on the Tauc plot. Photoluminescence Spectroscopy was recorded on an Edinburgh FLS1000 spectrophotometer equipped with a 150 W Xe-lamp as the excitation source. Room-temperature electron spin resonance (ESR) spectra of samples were collected on a Bruker EMXplus-6/1.

The in-situ Fourier transform infrared (FTIR) measurements for the adsorption of isopropanol and n-propanol on WO_3 and Bi-N/WO_3 photoanodes were carried out on a PerkinElmer Frontier spectrometer and the spectrum was collected at a resolution of 1 cm^{-1} from 4000 to 1000 cm^{-1}.

TEM and high-resolution TEM (HRTEM) images were obtained by TEM (Tecnai G2 F30, FEI). The aberration-corrected The Pt L-edge XAFS was performed with Si (111) crystal monochromators at the W1BL14 beamline by the Shanghai Synchrotron Radiation Facility (SSRF)

PEC performance for photoanodes

The PEC performance was performed on an electrochemical workstation (CHI760E), the electrolyte was 0.5 M Na_2SO_4 mixed with 0.1 M glycerol electrolyte with pH adjusted to 2 by H_2SO_4, the light source was a 300 W Xe lamp (CEL-PF300-T8) with an AM 1.5G filter, and the standard three-electrode configuration consisted of a working electrode (as-prepared photoanodes), a counter electrode (platinum foil) and a reference electrode (Ag/AgCl electrode).

Electrochemical impedance spectroscopy (EIS) was employed to determine the charge carrier mobility. EIS spectra were monitored with 5 mV AC voltage amplitude, where the frequency range was set to be 0.1-10^6Hz. The transient photocurrent response was performed without bias voltage under irradiation of a xenon lamp with an interval of 30 s for light on and off. Mott-Schottky (MS) curves were collected at the amplitude of 5 mV scanning from -0.5 V to 0.5 V (vs. Ag/AgCl) with a 1000 Hz frequency under dark condition.

The reversible hydrogen electrode (RHE) potentials were converted from the measured potentials according to the followed equation:

$$E_{RHE} = E_{Ag/AgCl} + E_{Ag/AgClvs.NHE} + 0.059 \times pH \quad (1)$$

where $E_{Ag/AgClvs.NHE}$ is 0.197 V at 25 °C.

The liquid products were evaluated by high performance liquid chromatography (HPLC; Agilent LC-1260) with an ultraviolet detector, a differential refractive index detector and an Aminex HPX-87H column (300 mm×7.8 mm×9 μm, Bio-Rad). The gaseous products were analyzed by gas chromatography (Fuli GC-9790II) with a thermal conductivity detector (TCD).

Selectivity of DHA was calculated by:

$$\text{Selectivity (DHA)} = c_{DHA}/(c_{DHA} + c_{GLD} + c_{GA} + c_{FA}) \times 100\% \quad (2)$$

DFT calculations

The Vienna ab initio Simulation Package (VASP) was used to conduct DFT calculations. [1] The Perdew-Burke-Ernzerhof (PBE) within the generalized gradient approximation (GGA) was applied to treat the exchange-correlation functional, and the projected augmented wave (PAW) was used to describe the electron-ion interaction. [2, 3] A cutoff energy of 500 eV was set for the plane-wave basis set. A Monkhorst-Pack grid of 2 × 2 × 1 was employed for Brillouin zone sampling [4]. The convergence criterion of the energy and force were set as 10^{-5}eV and 0.05 eV/Å. WO_3 exposed (0 0 1) facet was applied to construct corresponding calculation models with 20 Å vacuum thickness. The Bi-WO_3 model was constructed by replacing the W atomic site of WO_3 model with Bi atom. Bi,N-WO_3 was constructed by replacing O atom sites adjacent to Bi atom with

N atom in Bi-WO_3. The GOR process was calculated in the following four steps:

Step1: $* + C_3H_8O_3 \rightarrow *C_3H_8O_3$ $\Delta G1$

Step2: $*C_3H_8O_3 \rightarrow *C_3H_7O_3 + H$ $\Delta G2$

Step3: $*C_3H_7O_3 + H_2O \rightarrow *C_3H_8O_4 + H$ $\Delta G3$

Step4: $*C_3H_8O_4 \rightarrow *C_3H_6O_3 + H_2O$ $\Delta G4$

Where * represents the active sites on the surface of WO_3, Bi-WO_3 and Bi,N-WO_3, and $*C_3H_7O_3$ and $*C_3H_8O_4$ represent the intermediates adsorbed on the active sites.

Table S1 Bi element contents of different catalysts by ICP-OES measurements.

Samples	Bi content (wt%)
Bi-WO_3	0.16%
Bi,N-WO_3	0.16%

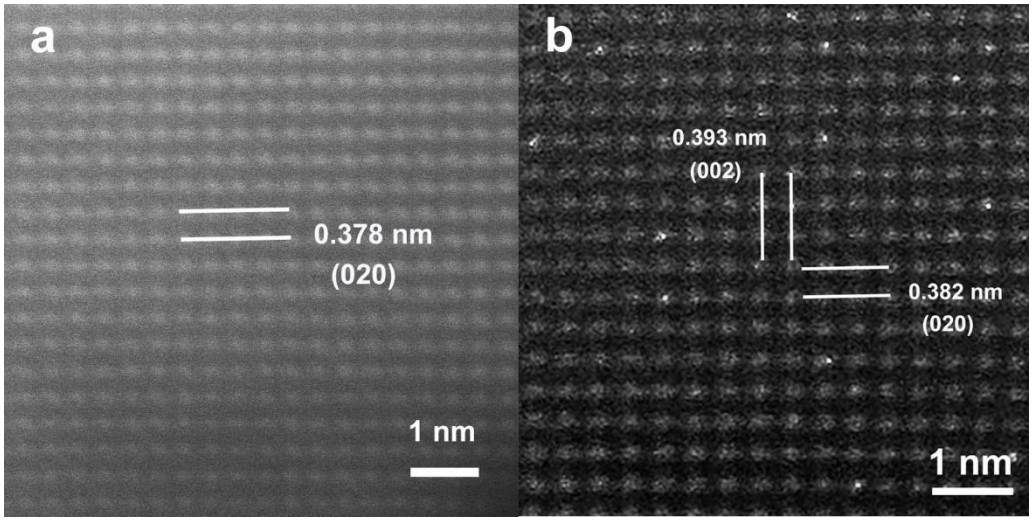

Figure S1. HAADF STEM images of WO_3 (a) and Bi,N-WO_3 (b).

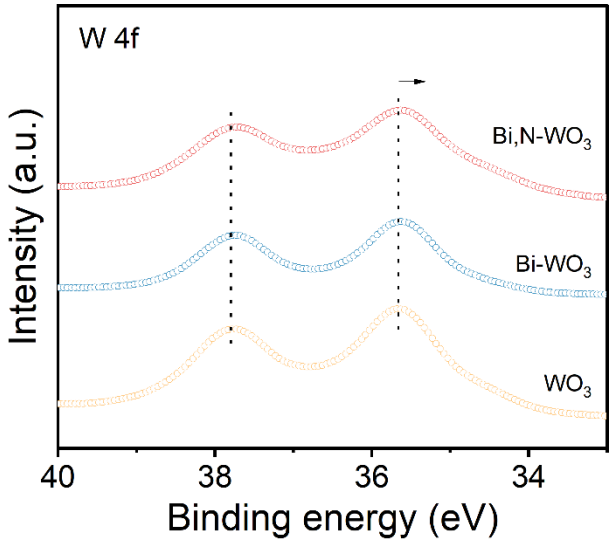

Figure S2. W 4f XPS spectra of Bi-WO_3, Bi,N-WO_3, Bi foil, and Bi_2O_3.

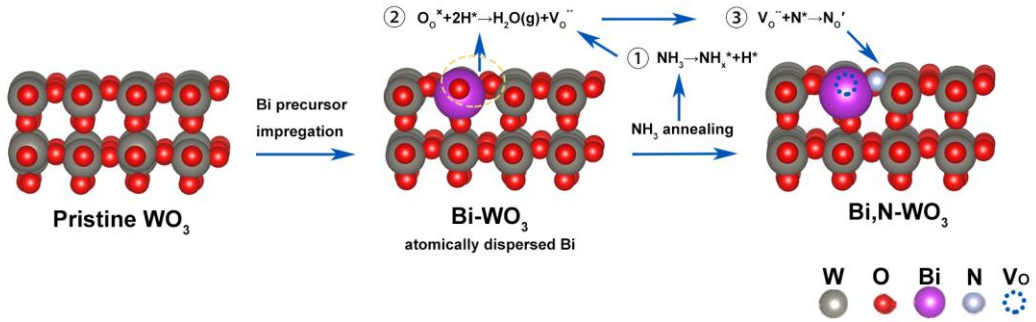

Figure S3. The schematic model of the proposed atomic-structure evolution.

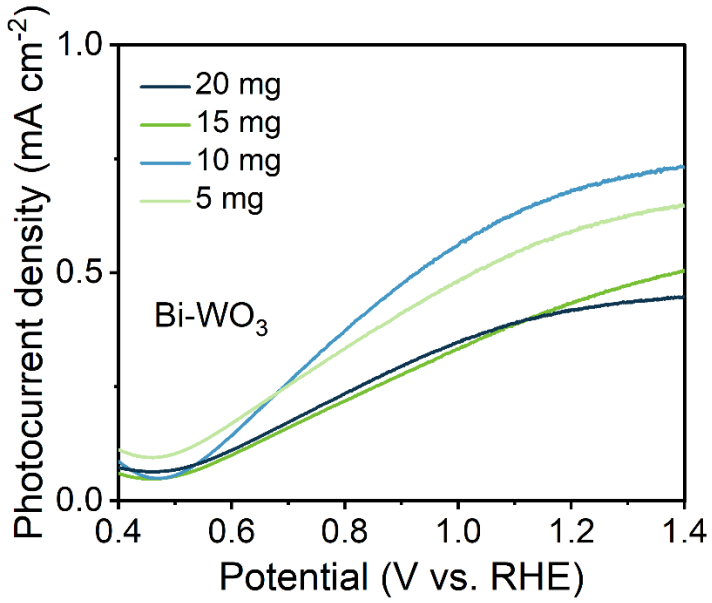

Figure S4. LSV curves of Bi-WO_3 photoelectrodes treated with different concentrations of a solution containing bismuth ions.

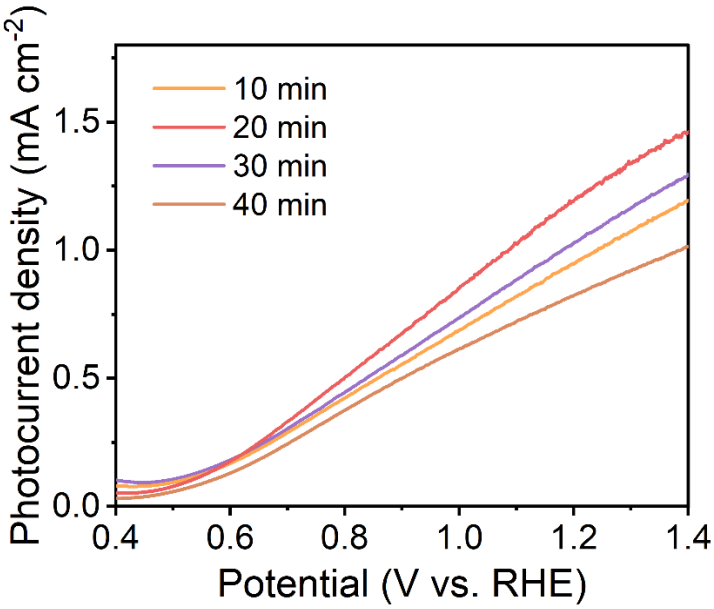

Figure S5. LSV curves of Bi,N-WO_3 photoelectrodes treated with different anneal time in 10%NH_3 atmosphere.

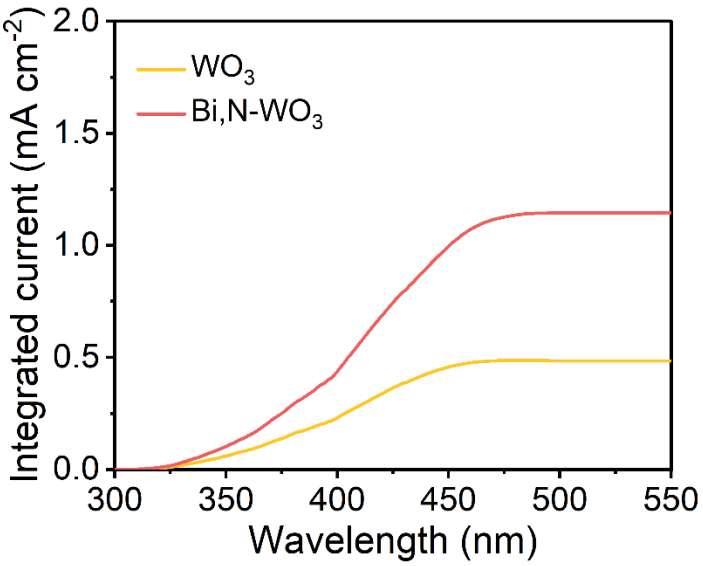

Figure S6. The corresponding integrated photocurrent density estimated from the IPCE curves.

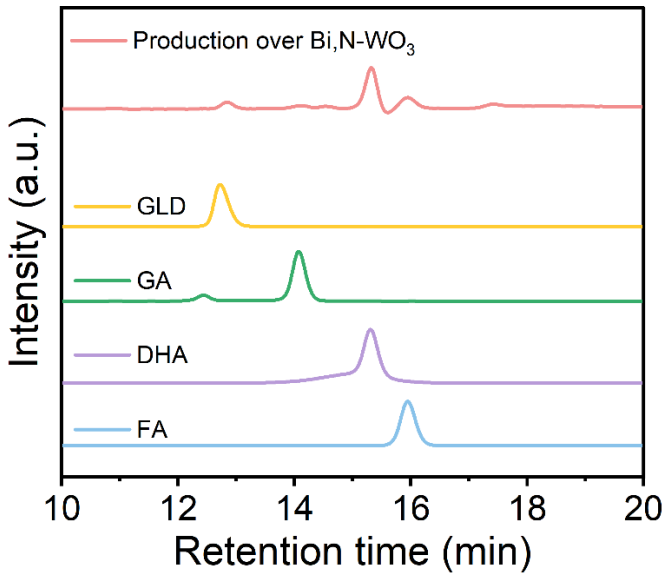

Figure S7. High performance liquid chromatography (UV detector = 210 nm) spectra of the PEC glycerol oxidation products over Bi,N-WO_3 photoanode for 1 h. (The yellow, green, purple and blue curves correspond to glyceraldehyde (GLD), glycolic acid (GA), dihydroxyacetone (DHA) and formic acid (FA), respectively)

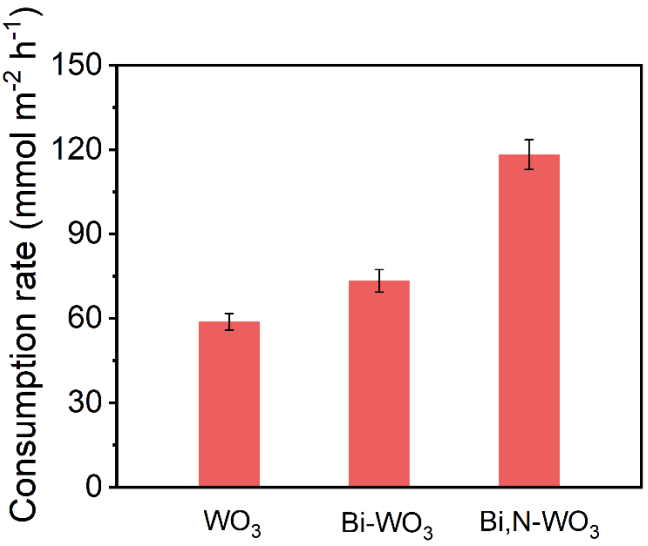

Figure S8. Consumption rate of glycerol over WO_3, Bi-WO_3 and Bi,N-WO_3 photoanodes.

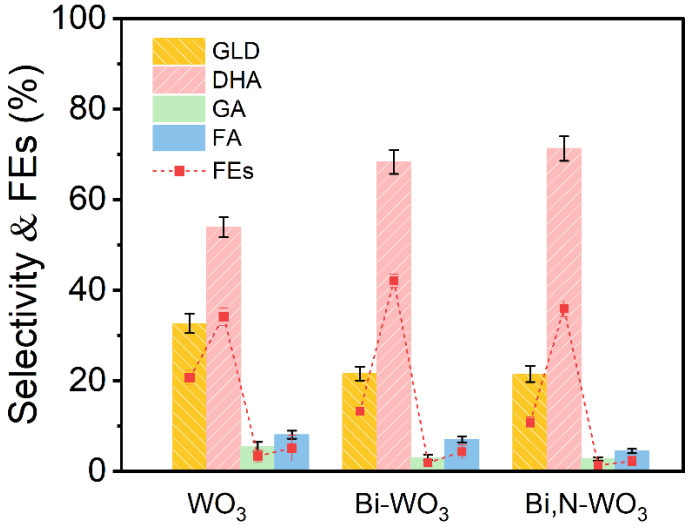

Figure S9. Selectivity and FEs of liquid products over WO_3, Bi-WO_3 and Bi,N-WO_3 photoanodes within 1h.

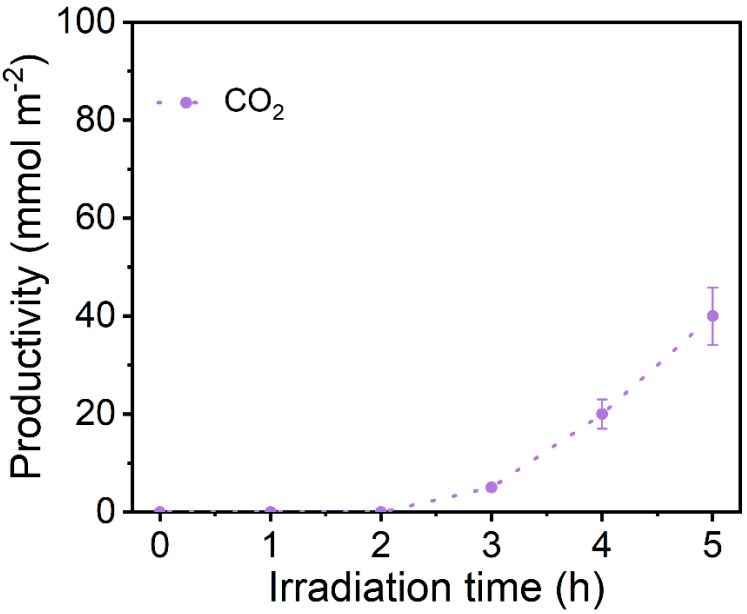

Figure S10. Productivity of products over Pt-SA/WO_x photoanode.

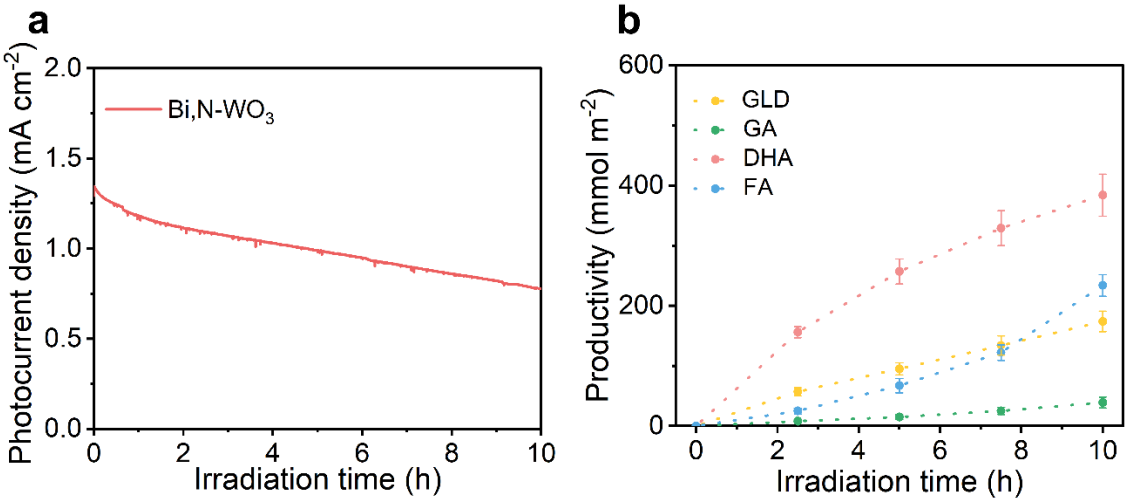

Figure S11. (a) I-t stability test of Bi,N-WO_3 photoanode measured at 1.2 V vs. RHE for 10 h. (b) Productivity of products in the Bi,N-WO_3tandem cell measured at 1.2 V vs. RHE for 10 h.

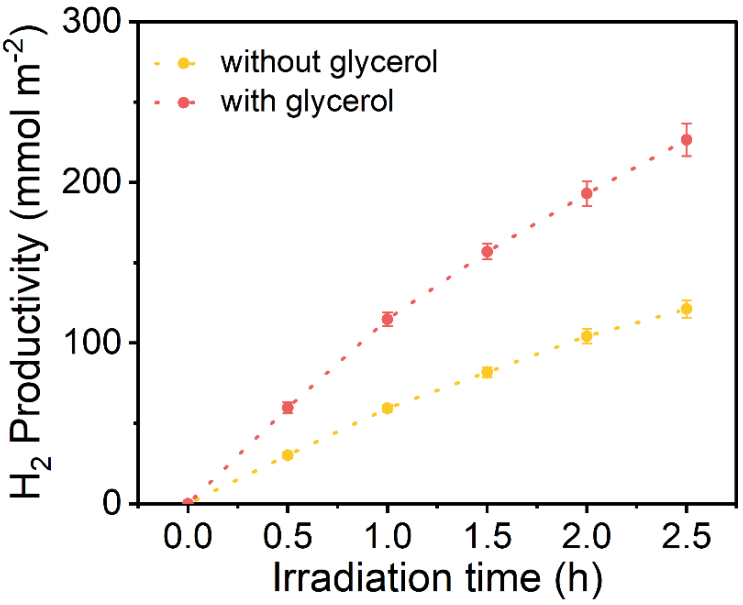

142

143 Figure S12. H_2 production with and without glycerol (Bi,N-WO_3 as photoanode).

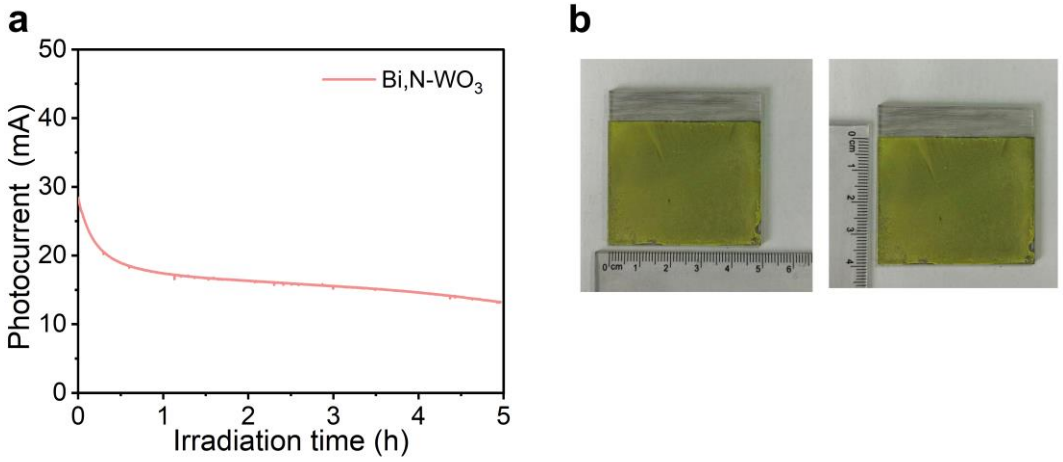

144

145 Figure S13. (a) I-t stability tests measured at 1.2 V vs. RHE for large-sized pristine

146 Bi,N-WO_3 photoanode. (b) Photographs of the the large size (5 × 4 cm^2) photoanode

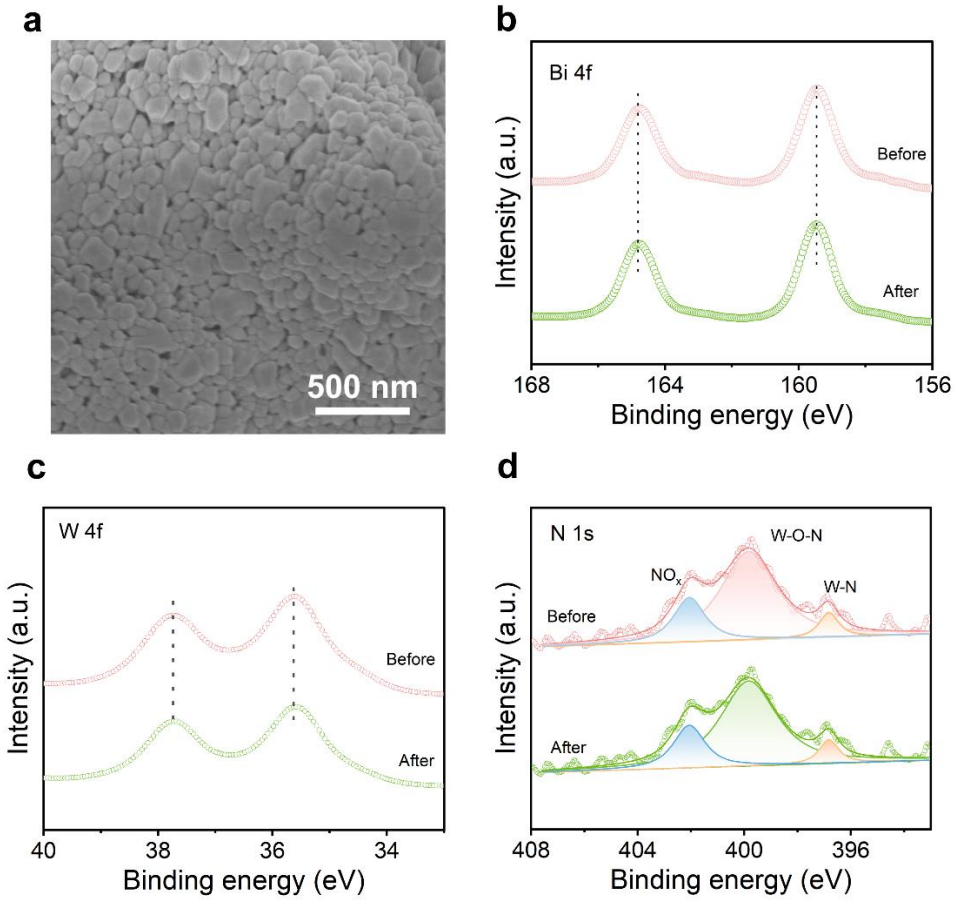

Figure S14. (a) Top-view SEM image, (b, c, d) XPS of Bi 4f, W 4f and N 1s for Bi,N-WO_3 after PEC.

Table S2. The EIS fitting result comparison of WO_3, Bi-WO_3 and Bi,N-WO_3.

Samples	R_s/Ω	R_{ct}/Ω	CPE/F
WO_3	3.97	82.86	1.75E-8
Bi-WO_3	4.38	63.16	1.29E-8
Bi,N-WO_3	4.11	52.40	2.27E-8

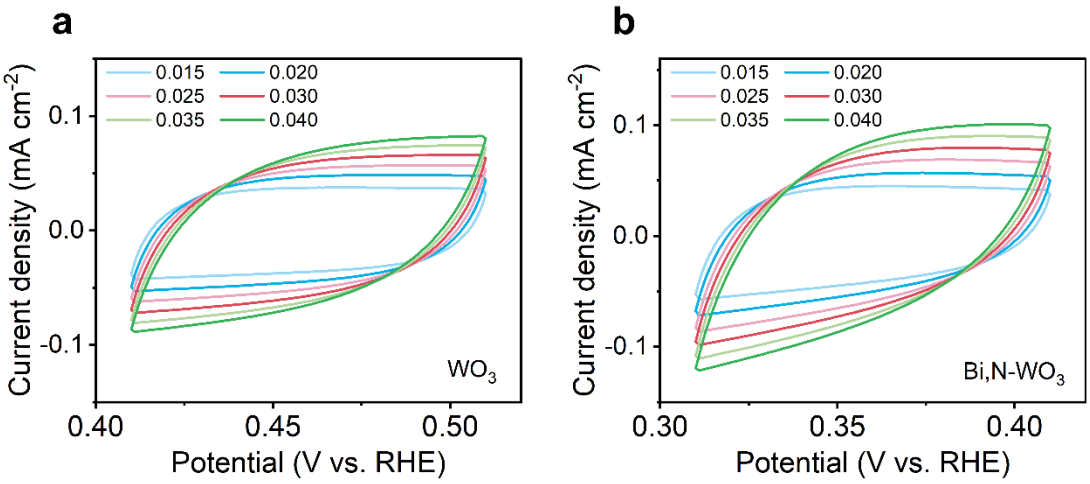

Figure S15. Cyclic voltammograms of a) WO_3 and b) Bi,N-WO_3 photoanodes were measured in a non-Faradaic region at the scan rates: 0.015, 0.020, 0.025, 0.030, 0.035, and 0.040 V s^{-1}.

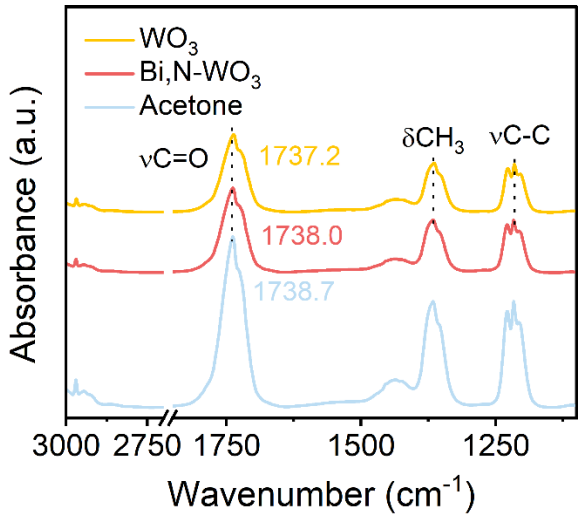

Figure S16. In situ FT-IR spectra of acetone over WO_3 and Bi,N-WO_3 after adsorption for 30 min followed by desorption for 20 min.

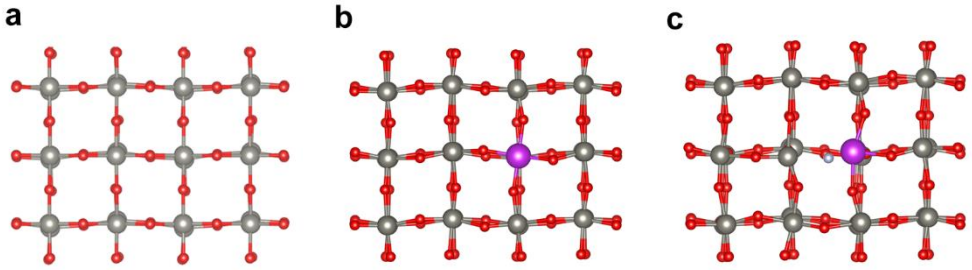

Figure S17. The computational models of WO_3 (a), Bi-WO_3 (b) and Bi,N-WO_3 (c). Grey represents W, red represents O, purple represents Bi, and white represents N.

Table S3. Comparison of Bi,N-WO_3 with other previously reported photoanodes for PEC glycerol oxidation reaction coupled with cathodic hydrogen generation.

Photoanode	Electrolyte	Potential	Target Product	Productivity	Selectivity	Ref.
$BiVO_4$	0.5 M Na_2SO_4 with 0.1 M glycerol (pH=2)	1.2 V vs. RHE	DHA	200 mmol m^{-2} h^{-1}	51%	5
{010}-$BiVO_4$	0.1 M $Na_2B_4O_7$ with 0.1 M glycerol (pH=2)	1.1 V vs. RHE	DHA	~9 μmol cm^{-2} h^{-1}	~60%	6
m-H-WO_3/TiO_2	0.5 M Na_2SO_4 with 0.1 M borate buffer and 0.1 M glycerol (pH=6)	1.2 V vs. RHE	GLD	~35.3 μmol cm^{-2} h^{-1}	~62.4%	7
α-Fe_2O_3	0.1 M KOH with 0.1 M glycerol (pH =12.9)	1.0 V vs. RHE	glycolate	3.13 mM cm^{-2} h^{-1}	~60%	8
Bi,N-WO_3	0.5 M Na_2SO_4 with 0.1 M glycerol (pH=2)	1.2 V vs. RHE	DHA	118.2 mmol m^{-2} h^{-1}	71.3%	This work

References

[1] G. Kresse, J. Furthmüller, *Phys. Rev. B* **1996**, 54, 11169-11186.

[2] P. E. Blöchl, *Phys. Rev. B* **1994**, 50, 17953-17979.
[3] J. P. Perdew, K. Burke, M. Ernzerhof, *Phys. Rev. Lett.* **1996**, 77, 3865-3868.
[4] H. J. Monkhorst, J. D. Pack, *Phys. Rev. B* **1976**, 13, 5188-5192.
[5] D. Liu, J. C. Liu, W. Cai, J. Ma, H. B. Yang, H. Xiao, J. Li, Y. Xiong, Y. Huang, B. Liu, *Nat. Commun.* **2019**, 10, 1779.
[6] T.-G. Vo, C.-C. Kao, J.-L. Kuo, C.-c. Chiu, C.-Y. Chiang, *Appl. Catal. B Environ.* **2020**, 278, 119303.
[7] Z. Gu, X. An, R. Liu, L. Xiong, J. Tang, C. Hu, H. Liu, J. Qu, *Appl. Catal. B Environ.* **2021**, 282, 119541.
[8] N. Perini, C. Hessel, J. L. Bott-Neto, C. T. G. V. M. T. Pires, P. S. Fernandez, E. Sitta, *J. Solid State Electrochem.* **2021**, 25, 1101-1110.